

# Quantized conductance in SnO<sub>2</sub> nanobelts

E R Viana\*, G M Ribeiro, J C González and A G de Oliveira

Departamento de Física, Instituto de Ciências Exatas, Universidade Federal de Minas Gerais,  
Av. Pres. Antônio Carlos, 1500, Pampulha, 31270-901, Belo Horizonte/MG – Brazil.

E-mail: [emilson.fisica@gmail.com](mailto:emilson.fisica@gmail.com); [emilsonfisica@ufmg.br](mailto:emilsonfisica@ufmg.br).

## Abstract

A single tin oxide (SnO<sub>2</sub>) nanobelt was connected in a back-gate field-effect transistor configuration. The device shows quantized conductance, in the form of a current staircase enhancement in the drain current vs. gate voltage characteristic curves. This current staircase, also called current oscillations, is attributed to successive filling of energy subbands by electrons, as a function of the applied gate voltage enhancement. Since the quasi-Fermi energy level ( $E_{\text{fermi}}$ ) increases along with the gate voltage, the channel conductance shows a step-change every time when  $E_{\text{fermi}}$  coincides with one subband edge. The origin of the subbands comes from the quantum confinement of the carriers, in the plane perpendicular to the transport direction. The oscillations could be identified and measured only for low values of temperature, between 6K and 50K, and for low values of the drain voltage  $V_{\text{ds}}$ , between 1 and 100mV, in a nanobelt with cross section dimensions approximately  $75 \times 175 \text{ nm}^2$ . We claim that the reported quantized conductance comes from the field-induced confinement that created conditions for the emergence of the “quantum wire” phenomena. In this way, at the present date our results show for the first time in SnO<sub>2</sub> nanobelts a fascinating quantum confinement effect in a material that is expected to behave as bulk in the absence of gate field.

(Some figures may appear in colour only in the online journal)

**PACS:** 73.63.Nm, 85.35.Be, 81.07.-b and 81.07.Vb

**Keywords :** tin oxide, nanobelt, FET, quantum wires, quantized conductance, electrical transport.

**Submitted to:** Nanotechnology (ISSN 0957-4484, ISSN 1361-6528)

---

## 1. Introduction

One dimensional nanostructures have stimulated significant contributions in scientific research in recent years, mostly due to interesting optical <sup>[1, 2]</sup> and electrical <sup>[3,4]</sup> properties, related to their structural dimensionality and to quantum confinement effects <sup>[5,6]</sup>.

Metal-oxides semiconductor nanostructures, such as tin oxide (SnO<sub>2</sub>) nanowires and nanobelts <sup>[7]</sup> have large potential for applications in gas <sup>[6-11]</sup> and ultraviolet light <sup>[12]</sup> sensors. Therefore, study of electrical transport in such nanostructures is very important in order to probe the low dimensionality and consequently quantum effects in nano-based devices.

The fundamental aspects of the electrical conduction mechanisms still remain unclear and challenging for the SnO<sub>2</sub> nanobelts and nanowires. Recently some authors have discussed the hard task of metal-oxide nanowires characterization <sup>[13,14]</sup>, due

to difficulties in obtaining ohmic contacts and to the environmental exposure <sup>[15]</sup>.

Since the functional oxides nanobelts can be used as an ideal system for a fully understand of the space-confined transport phenomena <sup>[7]</sup> so, in this work, SnO<sub>2</sub> nanobelts were synthesized, using the vapor-liquid-solid (VLS) method <sup>[16]</sup>, and the electrical transport studied.

The morphology and crystal structure of the as-synthesized SnO<sub>2</sub> nanobelts were analyzed and characterized by scanning electron microscopy (SEM), transmission electron microscopy (TEM), atomic force microscopy (AFM), and X-ray diffraction (XRD). The electrical transport study was carried out by connecting an individual nanobelt in a back-gate FET configuration (NB-FET) and measuring their properties as a function of temperature and gate voltage.

It will show that the SnO<sub>2</sub> NB-FET's exhibit source-drain current oscillations, quantized

conductance, induced by quantum confinement. The current oscillations fade out for source-drain voltages ( $V_{ds}$ ) larger than 100 mV, and temperatures higher than 50K. This suppression effect will be explained by simple theoretical and experimental models which take into account; the filling of consecutive subband energies by electrons, the temperature, and the applied gate voltage [17,18].

Despite of several different approaches developed to study confinement effects [5, 19-26], and ballistic transport in nanostructured materials [27,28], as far as we know, until the present date there is no report of the quantized conductance in  $\text{SnO}_2$  nanostructures that is present here.

## 2. $\text{SnO}_2$ nanobelts: synthesis and characterization

$\text{SnO}_2$  nanobelts were synthesized by using a gold-catalyst-assisted VLS method [16], that is a method based on thermal evaporation of oxide powders under controlled conditions. A suitable amount of pure Sn powder (1g, 99.99% purity) was placed on top of a Si: $\text{SiO}_2$  substrate of 1 x 2  $\text{cm}^2$ , previously coated with a 5 nm thick Au film that works as a catalyst. The substrate was placed inside of the horizontal quartz tube in a conventional tube furnace. The tube was firstly evacuated for 15 min, using a turbo-molecular vacuum pump to  $10^{-5}$  Torr, and then filled with pure argon. The furnace was then heated up to 800°C at a rate of 20°C/min, under a flux of argon. The temperature of 800°C was kept constant for 2-3 hours, and then the furnace was left to freely cool. At the end,  $\text{SnO}_2$  nanobelts were found on the substrate surface in a cotton-wool-like form. The morphology and crystal structure characterization of the synthesized  $\text{SnO}_2$  nanobelts was carried out by SEM, AFM, TEM, XRD.

Figure 1 shows some morphological and structural investigations of the nanobelts. SEM examinations, see figure 1.(a), reveal a large quantity of nanobelts with typical widths in the range of 50 to 500 nm, and lengths 5 to 50  $\mu\text{m}$ . TEM examinations, see figure 1.(b), show that the nanobelts presents a prismatic cross-section and are covered by a 10-20nm thick amorphous tin oxide layer. Both, XRD and selected area electron diffraction (SAED), shown in figure 1.(c) and 1.(d), confirm the tetragonal rutile structure of the nanobelts with lattice constants of  $a = b = 0.473 \text{ nm}$  and  $c = 0.318 \text{ nm}$  [29].

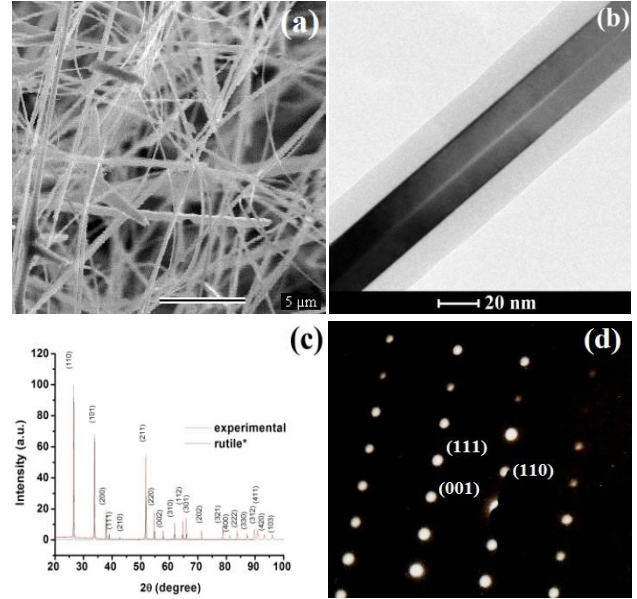


**Figure 1.** (a) SEM image of several  $\text{SnO}_2$  nanobelts, (b) TEM image of a prismatic  $\text{SnO}_2$  nanobelt covered by a thick amorphous layer, (c) XRD pattern of the nanobelts (red pattern) and the tetragonal rutile structure [6] (blue pattern), (d) SAED pattern of an individual nanowire.

## 3. Device fabrication

In order to prepare NB-FET devices, the  $\text{SnO}_2$  nanobelts were dissolved in deionized (DI) water by sonification and then deposited on a  $\text{SiO}_2/\text{Si}$  substrate. The substrate was previously cleaned by successive signification in trichloroethylene, acetone, isopropyl alcohol and DI water.

NB-FET were fabricated by photolithography using a LaserWriter® (UV-Laser,  $\lambda=405 \text{ nm}$ ), and standard lift-off process. A thermal evaporation of two-layer metallic electrodes consisting of a 10 nm of Cr followed by 150 nm of Au was used for the electrodes. The electrodes were 2-3  $\mu\text{m}$  apart and defined on top of a 300 nm thick  $\text{SiO}_2$ , deposited on a high-doped p-type Si substrate.

The  $\text{SnO}_2$  nanobelts are surrounded by an amorphous high resistivity oxide layer, so previously to the metal deposition, a  $\text{H}_2$ -plasma treatment was carried out in order to improve the quality of the contacts. The plasma treatment on the surface of  $\text{SnO}_2$  releases more charge carriers in the nanobelt conduction band, by the creation of oxygen vacancies and less coordinated tin species [30], and consequently an increase of the conductivity of the nanobelts is expected [30,31]. A schematic of the NB-FET is shown in figure 2, together with an AFM image of the actual device. Several devices were fabricated showing similar results and for this reason the data of only one device is presented here.

Four-contacts SnO<sub>2</sub> NB-FET device were fabricated, but only the two central contacts were used in the measurements presented in this work.

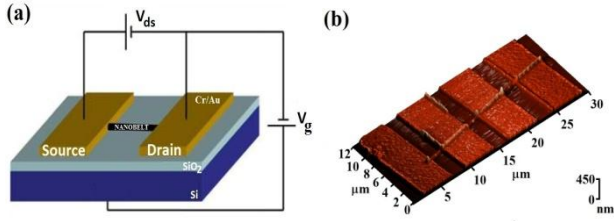


**Figure 2.** (a) Schematic back-gate FET-device used in this work. (b) AFM image of a NB-FET showing the 4 contacts on top of a SnO<sub>2</sub> nanobelt.

#### 4. Results

In order to study the electrical transport properties of the SnO<sub>2</sub> nanobelts the current  $I_{ds}$  was measured as a function of the source-drain voltage  $I_{ds}(V_{ds})$  and the gate voltage  $I_{ds}(V_g)$  for several temperatures  $T$ . The device was placed in a cold-finger He-7 cryostat, Oxford<sup>®</sup> CF1200, with a precise temperature-controller model Oxford<sup>®</sup> ITC503. A Keithley<sup>®</sup> 237 source meter was used to applied and record  $V_{ds}$  and  $I_{ds}$ , respectively.  $V_g$  was applied by a Keithley<sup>®</sup> 230 voltage source. Triaxial cable connections and guard system were used, in order to avoid wire capacitance and spurious resistances.

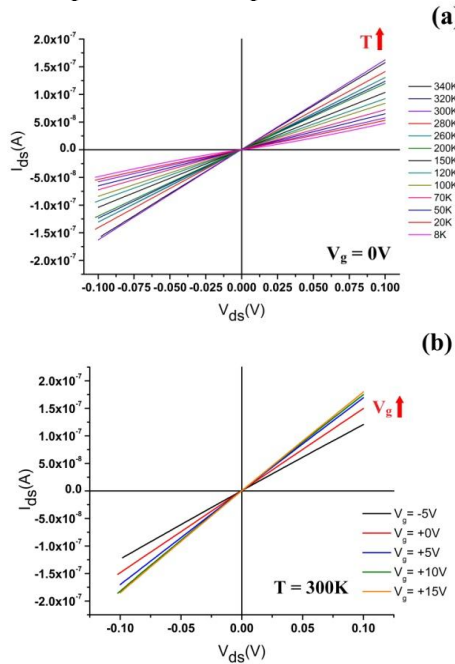


**Figure 3.** (a)  $I_{ds}$  curves as a function of temperature, with  $V_g = 0$  V. (b)  $I_{ds}$  curves as a function of  $V_g$  at  $T = 300$ K.

Figure 3 shows the  $I_{ds}(V_{ds})$  curves as a function of  $T$  and  $V_g$ . For these measurements  $V_{ds}$  was swap from  $-100$  mV to  $+100$ mV, in  $1$ mV steps. The linear behavior of the  $I_{ds}$  curves shows good ohmic contacts, and a transport dynamics mainly governed by the SnO<sub>2</sub> nanobelt conduction channel. Besides, the curves of figure 3.(a) show an increase of the conductance with temperature, as expect for a semiconductor material. The curves of figure 3.(b) show a reasonable field-effect-transistor behavior, that is, a transistor that relies on an electric field (gate) to control the shape, and hence the conductivity of a channel of charge carrier, in the semiconductor material.

Figure 4 shows the  $I_{ds}(V_g)$  curves as a function of  $V_g$  in the temperature range  $6.6$  to  $100$ K, with  $V_{ds} = 100$  mV. This curves show ohmic behavior with a shift of the threshold voltage ( $V_{th}$ ) towards more negative values, as the temperature increases. This behavior is the result of an increase in free carrier density with temperature<sup>[32]</sup>. At temperatures lower than  $50$  K some oscillations can be observed in those curves. This staircase behavior shows that at low temperatures the electrical transport in the NB-FET exhibits quantized conductance.

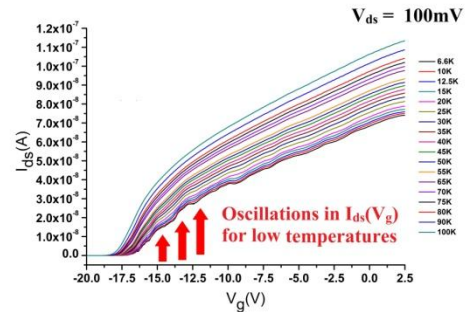


**Figure 4.**  $I_{ds}(V_g)$  curves as a function of temperature, in the  $6.6$  K to  $100$  K range, and under constant bias voltage  $V_{ds}=100$  mV. At low temperatures,  $T < 50$  K, a current staircase behavior is visible in the curves.

In figure 5 the  $I_{ds}(V_g)$  curves, at  $T = 6.6$  K, as a function of  $V_{ds}$  are presented. As  $V_{ds}$  increases the current steps are suppressed, showing that the confinement effects gradually vanishes. As it will be explained latter, the suppression of the current steps is a consequence of a increase of the electrons kinetic energy ( $q \cdot V_{ds}$ ) above the energy spacing between the bottom of the subbands energy in the conduction band of the SnO<sub>2</sub> nanobelts.

Similar quantum staircase behavior, also called oscillations in the  $I_{ds}(V_g)$  curves had already been observed in others nanodevices such as electron

gas<sup>[33]</sup>, quantum dots<sup>[26]</sup>, doublebarrier heterostructure devices<sup>[25,34]</sup>, silicon nanowires<sup>[21-22]</sup>, trigate MOSFET<sup>[5,18,19,20]</sup>, and, more recently, in graphene<sup>[27]</sup>. The oscillations are attributed to the successive filling of energy subbands by electrons as the gate voltage is increased, thereby enabling the experimental evaluation of the subband energy spacing in the electronic structure of the nanobelt, that refers to a “subband spectroscopy”<sup>[5]</sup>.

In NB-FET with a small cross section, conduction occurs in the innermost layer of the nanobelt. For values of  $V_g$ , below  $V_{th}$ , no conduction takes place from source to drain because of the “electrostatic squeezing”<sup>[28]</sup> of the conduction channel. For gate voltages just above the threshold, conduction is measured, and the carriers are confined within the filament conduction channel from source to drain. The filament cross section increases with the gate voltage, until the flat band is reached, that is when the filament cross section becomes equal to the physical cross section of the nanobelt<sup>[5,19]</sup>.

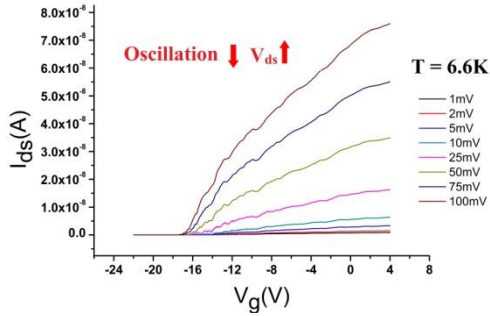


**Figure 5.**  $I_{ds}(V_g)$  curves as a function of  $V_{ds}$ , at  $T = 6.6$  K. Note the suppression of the current steps as  $V_{ds}$  increases.

The  $\text{SnO}_2$  nanobelt presented in figure 2.(b) has a prismatic cross-section of about  $75 \times 175 \text{ nm}^2$ , as measured from AFM, accounting for the crystalline plus the amorphous part. By solving an ideal 1D rectangular hard-potential, the electron energy levels, with respect to the bottom of the bulk conduction band, can be calculated as<sup>[18]</sup>:

$$E(k) = E_{yz} + E_x = E_{yz} + \frac{\hbar^2}{2m_x^*} k_x^2 \quad (2)$$

$$E_{yz} = \frac{\pi^2 \hbar^2}{2m_{y,z}^*} \left( \frac{n_y^2}{L_y^2} + \frac{n_z^2}{L_z^2} \right) \quad (3)$$

where  $E(k)$  gives the dispersion relationship of the energy subbands, and  $E_{yz}$  is the edge of the subbands. The indices  $n_y$  and  $n_z$  stand for the occupation numbers, and are defined by non-zero integers. The

effective mass of the electrons in  $\text{SnO}_2$  is  $m_{y,z}^* = 0.3m_o$ <sup>[30]</sup>, and  $L_y$  and  $L_z$  are the dimensions of the nanobelt cross-section.

For fixed  $n_z$ , we have almost degenerate subbands, with energies very close to each other, varying the parameter  $n_y$ . For this reason, the effective energy subband separation is mainly indexed by the parameter  $n_z$ . Under these conditions, the differences between the first three subband energy-levels,  $\Delta E_{theory} = [E_{yz}(1, n_z) - E_{yz}(1, 1)]$  are respectively 0.62, 1.80, and 3.35 meV. This three subband energy levels are expected to be measured, fixing  $n_y = 1$ , and varying  $n_z = 2, 3$  and 4, with respect to the ground state,  $E_{yz}(n_y = 1, n_z = 1) = E_{yz}(1, 1) = 0.264$  meV.

For an  $\Delta E_{theory}$  estimated larger than 3.35 meV, we have energy subbands indexed  $(n_y, n_z)$ , with  $n_y$  and  $n_z$  larger than 5, so that the amount of subbands become too high and we have a broad subband distribution. This explains why we could not visually detect conductance-steps for temperatures higher than about 50K, that corresponds to the thermal energy  $E_{thermal}$  of 4.3 meV.

The experimental energy separation,  $\Delta E_{exp}$ , between the first two subbands can also be estimated<sup>[17, 21, 22]</sup>, from the values of the gate voltage separation  $\Delta V_g$ , and the capacitance per unit area ( $C/A$ ) of the nanobelt, using the parallel-plane capacitor model :

$$\Delta E_{exp} = \frac{(C/A) \Delta V_g \cdot \hbar^2}{8\pi \cdot m^* \cdot e} \quad (4)$$

For  $\Delta V_g \approx 2.5 \text{ V}$ ,  $C = 1.6 \times 10^{-6}$  pF,  $m^* = 0.3m_o$ <sup>[30]</sup>, we have estimate the experimental subband energy separation  $\Delta E_{exp}$  approximately 0.8 meV. Equation (4) comes from the fact that the electron concentration obtained by the integration of the electron density of states, should be equal to that concentration induced by the applied gate voltage<sup>[17,21,22]</sup>.

The 0.8 meV value roughly compares with the first theoretical subband energy separation estimated  $\Delta E_{theory} = 0.62$  meV. So, the highest estimated subband separation energies, before we have a broad subband distribution, observable is  $(\Delta E_{theory})_{max} \approx 3.4$  meV. This energy leads to  $(T_{theo})_{max}$  of approximately 40K.

The estimated values  $\Delta E_{theory}$  and  $\Delta E_{exp}$ , using equation (3) and (4), are consistent with the fact that we only have quantized conductance, if the

thermal energy ( $k_B T$ ) is lower or comparable with the subband separation energies  $\Delta E$  [31]. That is, the temperature  $T$  must be lower than the estimated threshold-temperature  $(T_{\text{theo}})_{\text{max}} = 40\text{K}$ . Indeed, as presented in figure 4, conductance-steps are only observed for temperatures lower than around 50K.

The observation such oscillations is possible because the field induced carrier confinement, reinforced by the physical confinement, gives rise to well separated energy subbands. In such situation, as the quasi-Fermi energy level  $E_{\text{Fermi}}$  increases along with  $V_g$ , the channel conductance shows a step change every time  $E_{\text{Fermi}}$  coincides with a subband edge [5,21], and finally the current stair case looking like oscillations in the  $I_{\text{ds}}(V_g)$  curves can be observed. This explains why we could not visually detect conductance steps for temperatures higher than about 50K, that corresponds to the thermal energy  $E_{\text{thermal}}$  of 4.3meV.

## 5. Conclusions

The electrical transport mechanism of  $\text{SnO}_2$  nanobelts, synthesized via VLS method, was investigated by building, and characterizing, a single nanobelt in a back-gate field-effect transistor (NB-FET) configuration. The NB-FET shows space-confined transport phenomena, a field-induced quantized conductance in the form of oscillations in the current vs. gate voltage curves.

The oscillations were explained by filling of electron energy subbands as the gate voltage increases, since the quasi-Fermi energy level ( $E_{\text{fermi}}$ ) increases along with the gate voltage, the channel conductance shows a step-change, a oscillation, every time when  $E_{\text{fermi}}$  coincides with one subband edge. These oscillations could only be detected below a threshold-temperature of  $T_{\text{th}} = 50\text{K}$ , and for source-drain bias below 100 mV.

The energy separation between the first two subbands was experimentally estimated, using equation (4), to be of 0.8 meV. This value is in good agreement with theoretical calculations, using equation (3), that shows an energy separation between the first two subbands of 0.6 meV. We also show that before we get the broadband spectra (the hard-potential occupation numbers  $n_y$  and  $n_z$  lower than 5), we estimate a theoretical energy separation maximum,  $(\Delta E_{\text{theory}})_{\text{max}}$  of 3.4 meV, that corresponds to a temperature of 40K, that are also in agreement with the threshold-temperature  $T_{\text{th}}$  of 50K obtained from the experimental measurements.

Despite of several different approaches developed to study confinement effects [5, 19-26], and ballistic transport in nanostructured materials [27,28], as far as we know, until the present date there is no report of the quantized conductance in  $\text{SnO}_2$  nanostructures that was presented here.

## Acknowledgments

The authors' thanks Dr. Bernardo Ruegger Almeida Neves, and MSc. Ana Paula Barbosa for the presented AFM images. Dr. Nivaldo Lúcio Speziali for the XRD measurements. MSc. Além-Mar Bernardes Gonçalves and MSc. Marcos H. D. Guimarães, for invaluable discussion on transport measurements and device fabrication. Thanks CNPq, CAPES and FAPEMIG, Brazilian official agencies for funding this work.

## References

- [1] V. Lopez-Richard, J. C. González, F. M. Matinaga, C. Trallero-Giner, E. Ribeiro, M. Rebello Sousa Dias, L. Villegas-Lelovsky, and G. E. Marques 2009 *Nano Lett.* **9** 3129-3136.
- [2] J. C. González, M. I. N. da Silva, X. S. Lozano, D. Zanchet, D. Ugarte, E. Ribeiro, H. R. Gutiérrez, and M. A. Cotta 2006 *J. of Nanosci. Nanotechnol.* **6** 2182-2186.
- [3] Pai-Chun Chang, Jia Grace Lu 2008 *Appl. Phys. Lett.* **92** 212113.
- [4] A. M. B. Gonçalves, L. C. Campos, A. S. Ferlauto, R. G. Lacerda 2009 *J. of Appl. Phys.* **106** 034303.
- [5] Jong-Tae Park, Jin Young Kim, Chi-Woo Lee, Jean-Pierre Colinge 2010 *Appl. Phys. Lett.*, **97**, 172101.
- [6] Marion E. Frankie, Tobias J. Koplin, and Ulrich Simon 2006 *Small* **2**, 36-50.
- [7] Zheng Wei Pan, Zu Rong Dai, Zhong Lin Wang. 2001 *Science* **291** 1947-1949.
- [8] E. Comini, G. Faglia, G.Sberveglieri, Zhengwei Pan, and Zhong L. Wang 2002 *Appl. Phys. Lett.* **81** 1869.
- [9] L. L. Fields, J. P. Zheng, Y. Cheng, P. Xiong 2006 *Appl. Phys. Lett.* **88** 263102.
- [10] Yi Cheng, P. Xiong, C. Steven Yun, G. F. Strouse, J. P. Zheng, R. S. Yang, and Z. L. Wang. 2008 *Nano Lett.* **8** 4179-4184.
- [11] Q. Wan, Q. H. Li, Y. J. Chen, T. H. Wang, and X. L. He 2004 *Appl. Phys. Lett.* **84** 3654.
- [12] Cheng-Hua Lin, Reui-San Chen, Tzung-te Chen, Hsin-Yi Chen, Yang-Fang Chen, Kuei-Hsien Chen, and Li-Chyong Chen. 2008 *Appl. Phys. Lett.* **93** 112115.
- [13] Wang Z.L. 2003 *Adv. Mater.* **15** 432-436.
- [14] E. Schlenker, A. Bakin, T. Weimann, P. Hinze, D. H. Weber, A. Golzhauser, H-H Wehmann, and A Wang. 2008 *Nanotechnology*, **19** 365707.

- [15] Lao C.S., Liu J., Gao P., Zhang L., Davidovic D., Tummala R., and Wang Z.L. 2006 *Nano Lett.* **6** 263-266.
- [16] R. S. Wagner, W. C. Ellis 1964 *Appl. Phys. Lett.* **4** 89.
- [17] J.R. Gao, C. de Graaf, J. Caro, S. Radelaar, M. Offenbergh, V. Lauer, J. Singleton, T. J. B. Janssen, and J.A.A.J. Perenboom 1990 *Phys. Rev. B* **41** 12315-12318.
- [18] Nima Dehdashti Akhavam, Aryan Afzalian, Chi-Woo Lee, Ran Yan, Isabelle Ferain, Pedram Razavi, Giorgos Fagas, and Jean-Pierre Colinge 2010 *IEEE Trans. Electron Devices* **57** 1102-1109.
- [19] Jean-Pierre Colinge et. al. 2010 *Nat. Nanotechnol.* **5** 225.
- [20] Jean-Pierre Colinge, et. al. 2006 *IEEE Elect. Dev. Lett.* **27** 172-174.
- [21] Minkyu Je, Sangyeon Han, Ilgweon Kim, Hyungcheol Shin 2000 *Solid State Electr.* **44** 2207-2212.
- [22] Tang YS, Jin G, Davies JH, Williamson JG, Wilkinson CDW 1992 *Phys. Rev. B* **45** 13799-13802.
- [23] N.T. Bagraev, A. D. Buravlev, L. E. Klyachkin, A. M. Malyarenko, W. Gehlhoff, V. K. Ivanov, and I. A. Shelykh 2002 *Semiconductors* **36** 439-460.
- [24] A. T. Tilke, F. C. Simmel, H. Lorenz, R. H. Blick, and J. P. Kotthaus 2003 *Phys. Rev. B* **68** 075311.
- [25] Bo Su, V. J. Goldman, and J. E. Cunningham 1992 *Phys. Rev. B*, **46** 7644-7655.
- [26] L.P. Kouwenhoven, A. T. Johnson, N. C. van der Vaart, C. J. P. Harmans 1991 *Phys. Rev. Lett.* **67** 1626-1629.
- [27] Nikolaos Tombros, Alina Vergura, Juliane Junesch, Marcos H. D. Guimarães, Ivan J. Vera-Marun, Harry T. Jonkman, and Bart J. van Wees. 2011 *Nature Phys.* **7** 697-700.
- [28] D. A. Wahran, U. Ekenberg, M. Pepper, D. G. Hasko, H. Ahmed, J. E. F. Frost, D. A. Ritchie, D. C. Peacock, and G. A. C. Jones 1989 *Phys. Rev. B*. **39** 6283.
- [29] T. Yamanaka, R. Kurashima, J. Mimaki. 2000 *Z. Kristallogr.* **215** 424-428.
- [30] John Rovertson 1984 *Phys. Rev. B* **30** 3520-3522.
- [31] Juan Pan, Rajesh Ganesan, Hao Shen, Sanjay Mathur 2010 *J. Phys. Chem. C* **114** 8245-8250.
- [32] E. J. Boyd, and S.A. Brown 2009 *Nanotechnology* **20** 425201.
- [33] B. J. van Wees, et.al. 1988 *Phys. Rev. Lett.* **60** 848-850.
- [34] E. Kapon, D. M. Hwang, and R. Bhat 1989 *Phys. Rev. Lett.* **63** 430.